5782 *Biochemistry* **2010,** *49,* 5782–5789
DOI: 10.1021/bi100634h

BIOCHEMISTRY
including biophysical chemistry & molecular biology
Article

Acridine−N Peptide Conjugates Display Enhanced Affinity and Specificity for boxB RNA Targets[†]

Xin Qi,[‡,∥] Tianbing Xia,[‡,⊥] and Richard W. Roberts*[,‡,§]

[‡]*Division of Chemistry and Chemical Engineering, California Institute of Technology, 1200 East California Boulevard, Mail-code 147-75, Pasadena, California 91125, and* [§]*Department of Chemistry, Chemical Engineering, and Biology, University of Southern California, 507 RTH, Los Angeles, California 90089-2905.* [∥]*Present address: The Scripps Research Institute-Florida, 130 Scripps Way, Jupiter, FL 33458.* [⊥]*Present address: Department of Molecular and Cell Biology, The University of Texas at Dallas, Richardson, TX 75080-3021.*

Received April 25, 2010; Revised Manuscript Received June 7, 2010

ABSTRACT: Arginine-rich peptides and small-molecule intercalating agents utilize distinct molecular mechanisms for RNA recognition. Here, we combined these distinct binding modules in an effort to create conjugate ligands with enhanced affinity and specificity using the bacteriophage λ N peptide−boxB interaction as a model system. We first designed and synthesized a series of peptide−acridine conjugates using portions of the RNA-binding domain of N protein (11- and 22- residue peptide segments) and then compared the binding affinity, specificity, salt dependence, and structural properties of the RNA−peptide and RNA−peptide−acridine conjugate complexes using steady-state fluorescence, CD spectroscopy, NMR, and native gel mobility shift assays (GMSAs). These analyses revealed that the full-length peptide−acridine conjugate displayed substantially improved RNA binding affinity (∼80-fold; $K_d \sim 15$ pM) relative to that of the peptide alone ($K_d \sim 1.2$ nM). In accordance, we also observed specificity enhancement (∼25-fold) as determined via comparison of the binding of the best conjugate to a cognate λ boxB RNA with that to a noncognate P22 RNA hairpin (80-fold vs 3.2-fold enhancement). Furthermore, the observed binding enhancement was unique to the full-length conjugate with a flexible linker, implying that the structural context of the acridine presentation was critical. Taken together, our observations support the idea that peptide- and intercalation-based binding can be combined to create a new class of high-affinity, high-specificity RNA-binding ligands.

The design of proteins and other ligands with the capacity to recognize nucleotide sequences with high affinity and specificity has been the subject of extensive research in recent years; for example, designed novel zinc finger proteins (*1*−*3*) and polyamides (*4*−*7*) were found to target the major and minor groove of DNA, respectively. In comparison, RNA molecules often fold into complex and unique three-dimensional shapes and perform versatile functions in diverse biological processes, thus prompting great interest in designing sequence- or structure-specific RNA-binding molecules. Enhanced understanding of sequence-specific RNA-binding molecules and the expanding structural databases for RNA and RNA−protein complexes, together with the development of new synthetic tools, have provided new opportunities for the design of peptide or small-molecule RNA binders.

One approach to achieving enhanced RNA binding is to combine different binding modules for interaction sites that coexist in a given RNA molecule. In principle, if two binding sites are in the proximity of each other, a dimeric derivative ligand can bind simultaneously to the two sites, resulting in a binding affinity greater than that of either module alone (*8*, *9*). Furthermore, such modular design of RNA-binding ligands has been successfully developed as multivalent ligands for targeting triplet repeat RNAs that are implicated in myotonic muscular dystrophy and shown to inhibit the formation of RNA−protein complexes (*10*).

As proof of principle, recent studies have shown acridine derivatives to be a useful intercalating module (*11*−*14*). In a new class of HIV-1 Tat[1] antagonists, a Tat−TAR binding inhibitor consisting of a substituted acridine and a polyamine moiety was demonstrated to inhibit Tat function (*15*). Specifically, the modular design principle was based on the stacking ability of the aromatic moiety of acridine and the contacts with the TAR RNA phosphate backbone by a polycationic anchor. The two modules are linked by an aliphatic linker. Aside from the compound stacking between two bases, direct hydrogen bond contacts with a G·C base pair were also involved.

Two other studies further illustrate the utility of acridine modules in RNA binding. A series of cationic small molecules were synthesized, and their abilities to bind defined RNA duplexes with and without bulged bases were investigated (*16*, *17*). Complex stabilization and selectivity for an RNA duplex containing a single bulged base over a normal RNA duplex have been obtained with a ligand consisting of a chloroacridine moiety covalently attached to 2,6-diaminopurine through an aminoalkyl linker. It is believed that the chloroacridine moiety intercalates into the RNA duplex and the 2,6-diaminopurine interacts with the bulged base. Another example of this type of binding enhancement is illustrated by a neomycin−acridine conjugate, synthesized by covalently linking neomycin B to 9-aminoacridine via a short spacer, as a potent inhibitor of Rev-RRE binding (*18*). Its affinity for the RRE is ∼50-fold higher than that of the parent

[†]This research is financially supported by National Institutes of Health Grant GM60416 (R.W.R.).

*To whom correspondence should be addressed. E-mail: richard.roberts@usc.edu. Phone: (213) 821-4132. Fax: (213) 421-4207.

[1]Abbreviations: TAR, trans-activating response region; Tat, trans-activators of transcription; Nut, N-utilization; 2AP, 2-aminopurine.

 Published on Web 06/08/2010

neomycin B and approaches that of the Rev peptide. These results demonstrate that the combination of different binding modes (e.g., ionic and intercalation) within one ligand is a powerful approach to enhancing RNA binding.

Acridine conjugation has also been used in designing functional molecules. For example, attachment of an acridine moiety to a catalytic tripeptide produced a RNase mimic (*19*), and that to a base linker construct generated abasic site recognition and cleavage functions (*20*). Acridine has also been used in conjunction with an oligonucleotide to facilitate site-selective RNA hydrolysis (*21*), where acridine was hypothesized to push the bulged base out of the helix and present a scission site.

In light of the versatile and modular functions of acridine, we reasoned that the same principle may also apply to the N peptide–boxB RNA complex system. Bacteriophage N proteins play an essential role in transcriptional antitermination, which is critical for phage development (*22*). The inhibition of transcription termination at both intrinsic and Rho-dependent terminators by N proteins depends on recognition of a cis-acting RNA element called Nut (N utilization) on the nascent phage transcript. Together with four *Escherichia coli* host factors (NusA, NusB, NusG, and ribosomal protein S10), N protein and Nut initiate the formation of a ribonucleoprotein complex that converts the RNA polymerase into a termination-resistant form (*22*, *23*).

The Nut site consists of a 5′-single-stranded RNA element (boxA) and a 3′ hairpin (boxB) (*24*, *25*). The boxB from λ phage is a 15-mer RNA stem–loop hairpin containing a purine-rich pentaloop. The RNA-binding domain of the N protein consists of an arginine-rich motif located at the N-terminus (*26*). The 22-residue short peptide recognizes the cognate boxB RNA with specificity and affinity similar to those of the intact N protein (*27*). Upon formation of the complex, four of the pentaloop nucleotides adopt a canonical GNRA tetraloop fold (*28*) with the fourth adenine extruded (*29*, *30*); the peptide forms a bent α-helix and binds tightly to the major groove of the RNA (*29*–*31*).

The RNA–protein interface of the λ_{N22}–boxB complex is dominated by electrostatic interactions and hydrophobic contacts (*29*). The five arginines and two lysines of λ_{N22} create a positively charged surface on one face of the α-helix that interacts with the negatively charged phosphodiester backbone of the boxB RNA. Hydrophobic interactions are also important for boxB recognition. Ala-3 and Trp-18 are involved in crucial hydrophobic interactions. In addition, the roles of arginine and lysine residues are not restricted to ionic interaction; some of the aliphatic portions of these side chains also contact the RNA bases or sugars.

Given the detailed characterization presented above, the λ_{N22}–boxB complex is an ideal model system for testing new binding modes, e.g., intercalation. In this paper, we report the use of acridine–peptide conjugates to enhance binding of boxB RNA targets by the N peptide.

MATERIALS AND METHODS

Synthesis of Peptides and Acridine–Peptide Conjugates. Crude peptides with or without linkers were constructed by automated solid phase peptide synthesis using Fmoc-protected monomers (ABI) on an Applied Biosystems 432A peptide synthesizer. A series of full-length λ_{N22} and truncated λ_{N11} acridine–peptide conjugates were manually synthesized on the resin using the chemistry outlined in Scheme 1. Two types of flexible linkers, a Gly-Gly linker and an ethylene glycol linker, were used.

Scheme 1: Synthesis and Quantification of Acridine–Peptide Conjugates

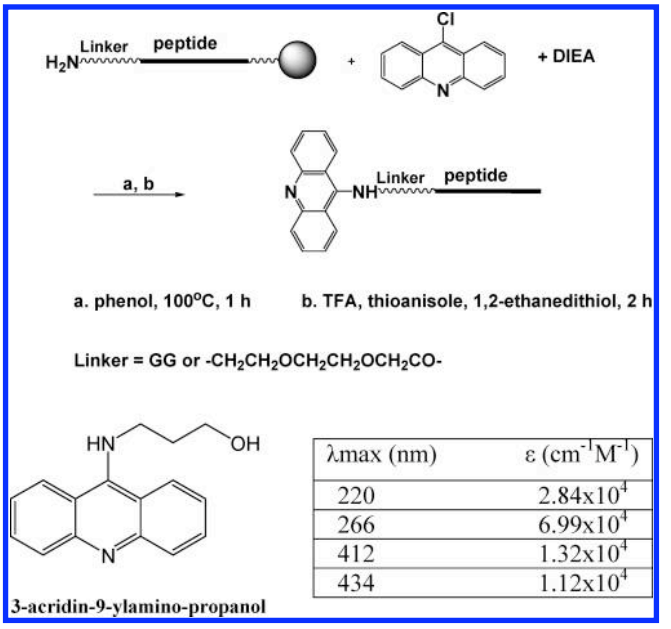

λmax (nm)	ε ($cm^{-1}M^{-1}$)
220	2.84×10^4
266	6.99×10^4
412	1.32×10^4
434	1.12×10^4

Crude peptides and crude acridine–peptide conjugates were deprotected and cleaved from the resin and purified by reverse-phase HPLC on a C18 column. The purity of the products was checked by analytical HPLC and their identity confirmed by MALDI-TOF mass spectrometry. Concentrations of peptide stocks were determined by UV absorption at 280 nm for free peptides containing either tryptophan or tyrosine, or at 412 and 434 nm for acridine–peptide conjugates using extinction coefficients ($\varepsilon = 1.32 \times 10^4$ cm^{-1} M^{-1} at 412 nm, and $\varepsilon = 1.12 \times 10^4$ cm^{-1} M^{-1} at 434 nm) determined for a water-soluble acridine derivative (3-acridin-9-ylaminopropanol) synthesized from 9-chloroacridine and 3-amino-1-propanol as described previously (*18*).

Synthesis of 2AP-Labeled RNA Oligomers. Crude RNA oligomers with a fluorescent 2-aminopurine (2AP) label substituted for adenine at the second, third, and fourth base positions of the pentaloop (denoted 2AP-2, 2AP-3, and 2AP-4, respectively) were constructed by automated synthesis using 2-aminopurine-TOM-CE phosphoramidite (Glen Research, Sterling, VA). Oligomers were deprotected and purified by 20% urea-PAGE. Purified oligomers were desalted on a NAP-25 column and quantified by UV absorption at 260 nm.

Steady-State Fluorescence Measurements. Steady-state fluorescence measurements were taken on a Shimadzu RF-5301PC spectrofluorophotometer as described previously (*27*, *32*). Aliquots of concentrated stocks of the free peptide or acridine–peptide conjugates were added stepwise to a stirred solution of 2AP-containing RNA maintained at various temperatures under a series of buffer conditions. The fluorescence signal of 2AP was monitored at 370 nm with excitation at 310 nm. Dissociation constants (K_d) were calculated for a one-step binding mechanism by nonlinear least-squares regression using DynaFit (*33*), as previously reported (*34*).

Band Shift Analysis. Free boxB RNA or peptide–RNA complexes were created in NMR buffer [50 mM NaCl, 10 mM phosphate, and 0.5 mM EDTA (pH 6)] and diluted with TBE buffer before being loaded onto a 20% nondenaturing PAGE gel maintained at 10–15 °C. Free RNA and complex bands were visualized by UV.

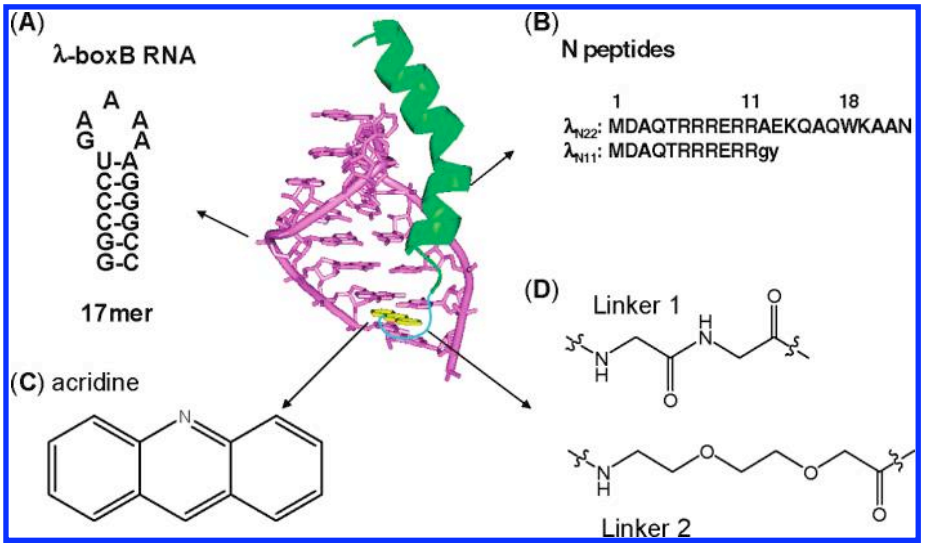

FIGURE 1: Design of the acridine−peptide conjugate binding to boxB RNA. Shown in the middle is the NMR structure (Protein Data Bank entry 1QFQ) of the boxB RNA−N peptide complex drawn with Pymol. The coordinates of the acridine moiety were modeled around the stem region for schematic purposes. (A) Sequences and secondary stem−loop structures of boxB RNA from λ bacteriophages used in this study. (B) Sequences of λ_{N22} full-length and truncated λ_{N11} peptides. The 11-mer was tagged with gy for quantification purposes. (C) Structure of acridine. (D) Structures of linkers.

One-Dimensional (1D) NMR Spectroscopy. Unlabeled 15-mer boxB RNA [5′-GCCCUGAAAAAGGGC-3′ (bases in the loop are underlined)] was synthesized by in vitro transcription using T7 RNA polymerase (*35*). The RNA was purified by 20% urea-PAGE and desalted on a NAP-25 column. Purified RNA oligomer was resuspended in NMR buffer [50 mM NaCl, 10 mM phosphate, and 0.5 mM EDTA (pH 6) in a 90:10 H_2O/D_2O mixture]. Spectra were recorded on a Varian INOVA 600 MHz NMR spectrometer at 25 °C. The spectrum of free boxB RNA was recorded first; titration of the concentrated peptide or acridine−peptide conjugate into the boxB RNA was monitored by inspection of the imino proton region of RNA.

CD Spectroscopy. Spectra were recorded on an Aviv 62 DS CD spectrometer at 20 °C. The samples contained 5 μM RNA and 6 μM peptide in 10 mM potassium phosphate buffer (pH 7.9). The spectra of the bound peptides were determined via subtraction of the spectra for free RNA and excess free peptide from that of the complex.

RESULTS

In the acridine−peptide conjugate−RNA complex, the high-affinity λN peptide is expected to bind to the major groove of the boxB RNA with the same molecular interactions as in the wild-type complex (*29*, *30*). Consequently, the acridine moiety may be positioned proximal to the lower part of the RNA stem where it can either intercalate into the stem (Figure 1) or simply associate with the RNA extrahelically.

K_d Values. Dissociation constants (K_d) were determined by monitoring the change in the fluorescence of 2-aminopurine (2AP) incorporated at variable positions within the loops of the RNA hairpins. This base was found to be an extremely useful probe for nucleic acid structure and dynamics (*36*), as well as RNA−peptide interactions (*32*). The fluorescence intensity of 2AP is highly sensitive to the local environment, exhibiting a decrease or increase when stacked or solvent-exposed, respectively (*37*). In most cases, peptide binding of the RNA can be detected by either a fluorescence increase or decrease of more than 20% from the starting value for the free boxB RNA (*27*, *38*).

Table 1 lists the K_d values directly determined at 50 mM K^+ and 20 mM Tris for acridine−λ_{N11} and acridine−λ_{N22} peptide conjugates, compared to those of WT peptides alone, for boxB RNA targets from both the λ and P22 phages. Binding affinities for truncated λ_{N11} peptide−acridine conjugates constructed with either a Gly-Gly linker **1** or an ethylene glycol linker **2** were similar and slightly weaker than those of the WT λ_{N11} peptide. However, the binding affinities were enhanced when the longer and more flexible linker **2** was used on the full-length peptide. The enhancement was dependent on the actual construct and RNA targets, and the conjugates displayed increased binding specificity. For example, an acridine−full-length peptide conjugate showed an affinity of 0.015 nM for the 17mer boxB RNA with 2AP-4 labeling when extrapolated from a high-salt measurement to 50 mM K^+ (Table 2 and Figure 2), corresponding to an 80-fold enhancement over that of the wild-type full-length peptide (1.2 nM). The longer and more flexible linker **2** seemed to confer affinity enhancement. Full-length acridine peptide conjugates constructed with the shorter and more rigid linker **1** exhibited less binding enhancement; therefore, further investigations were focused on linker **2**. In line with this view, we also observed specificity enhancement (~25-fold) determined via comparison of the enhanced binding affinity of the acridine−linker **2**−λ_{N22} peptide conjugate to a cognate λ boxB RNA (80-fold) with a modest enhancement (3.2-fold by comparing 257 nM with 80 nM) to a noncognate P22 RNA hairpin.

Salt Dependence of Binding. In general, protein−nucleic acid interactions become weaker with an increasing salt concentration due to the electrostatic nature of binding. This principle likely also applies to our system. Since the N peptide is arginine-rich, the electrostatic interactions between positively charged peptide side chains and the negatively charged RNA phosphate backbone are critical for binding (*29*). Consequently, these electrostatic interactions are mitigated by an increasing concentration of salt. Within a range of cation concentrations, plots of $\log(K_d)$ versus $\log[M^+]$ give a linear relationship. The slope of these plots corresponds to the number of counterions that are released upon peptide binding. In general, the slope is related to the net charge of the peptide and ranges from 2.5 to 5 for the N peptide sequences

Table 1: Dissociation Constants (K_d) for Peptides and Acridine−Peptide Conjugates against boxB_R RNA[a]

	λ boxB_R RNA targets (17mers)			P22 BoxB RNA
	λ-2AP-2	λ-2AP-3	λ-2AP-4	2AP-2
	A A A G A U A C G C G C G G C g c	A A A G A U A C G C G C G G C g c	A A A G A U A C G C G C G G C g c	C A A G A U A C G G C C G G C g c
Peptide	K_d (nM)	K_d (nM)	K_d (nM)	K_d (nM)
λ_{N11}	1126	1480	1000	
Acr-Link1-λ_{N11}	3945	2304	3504	
Acr-Link2-λ_{N11}	3082	2200	3245	
λ_{N22}	1.9	1.0	1.2	257
Acr-Link1-λ_{N22}	2.7	1.3	2.0	
Acr-Link2-λ_{N22}	0.025[b]	0.019[b]	0.015[b]	80

[a]Binding constants were determined for the standard condition: 20 °C, 50 mM KOAc, 20 mM Tris-OAc, pH 7.5. Individual isotherms were fit to a one-step reaction with an error of <10%. Hairpin base positions substituted with 2AP are underlined. Acr refers to the acridine moiety. [b]Extrapolated from the high-salt measurement to 50 mM K^+ (see Table 2 and Figure 2).

Table 2: Salt Dependence[a]

	λ boxB_R RNA target λ-2AP-4(17mer)							
	A A A G A U A C G C G C G G C g c							
	Total monovalent cation concentration (mM)							
Peptide	70	95	120	175	220	320	420	620
	K_d (nM)							
λ_{N22}	1.2	1.9	4.2	8.5	19.8	43.5		
Acr-Link2-λ_{N22}					0.5	1.1	2.1	10

[a]The total monovalent cation concentration is the sum of K^+ and Tris. Binding constants were determined for the standard condition: 20 °C, 50−600 mM KOAc, 20 mM Tris-OAc, pH 7.5. Individual isotherms were fit to a one-step reaction with an error of <10%. Hairpin base positions substituted with 2AP are underlined. Acr refers to the acridine moiety.

that have been tested (*34*). Representative salt-dependent curves of dissociation constants for the acridine−full-length N peptide conjugate−boxB RNA complex were shown using the 17-mer RNA with 2AP-4 labeling (Table 2 and Figure 2). Most of the isothermal curves showed biphasic transitions, with the second transition starting after the peptide conjugate reaches a 1:1 stoichiometry with the RNA target. The K_d values were fit to the first transition. Indeed, a higher salt concentration decreased the binding affinity of acridine−peptide conjugate for boxB RNA as observed for the WT peptide. The salt dependence graph shows the linear relationship at higher salt concentrations (Figure 2) as observed previously (*39*, *40*). The derived slope value of 2.9 was slightly higher than the value of 2.4 for the

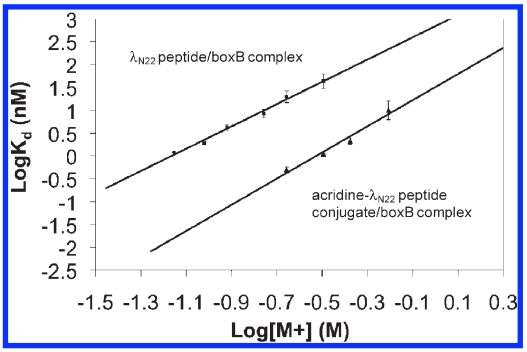

FIGURE 2: Salt dependence of the λ full-length peptide (■) and acridine−full-length peptide conjugate (▲) binding to 17-mer λ boxB RNA (2AP-4). Measurements were taken at 20 °C.

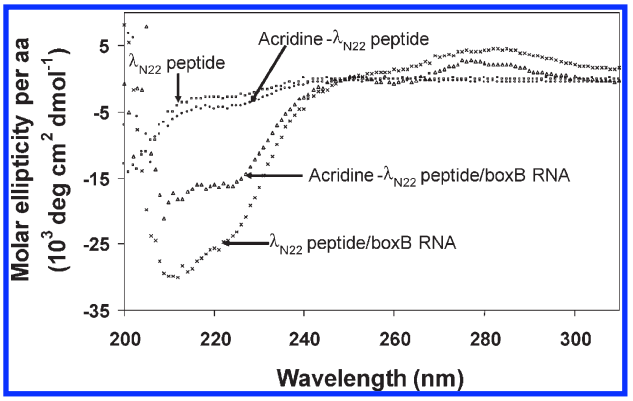

FIGURE 3: Comparison of CD spectra of free peptides and peptide−boxB RNA complexes.

wild-type N peptide, indicating roughly three cations were released upon binding. The K_d value extrapolated by the salt dependence curve to 50 mM K^+ and 20 mM Tris was 0.015 nM. A roughly 80-fold binding enhancement was observed across a broad range of ionic concentrations. Since the conjugate showed a slightly higher slope of salt dependence than the free peptide, the enhancement was even higher when extrapolated to lower salt concentrations.

CD Spectra. The CD spectra recorded for boxB RNA binding by the acridine−linker **2**−λ_{N22} peptide conjugate and free full-length λ_{N22} peptide are shown in Figure 3. Neither the peptide nor the acridine−peptide conjugate showed any appreciable structure in the absence of RNA. The difference spectra of the two complexes indicated that both peptides folded into α-helices when bound to the RNA. Although globally similar, the two complexes displayed specific differences in regions indicative of peptide folding (200−225 nm) and RNA folding (260−300 nm). The acridine conjugate−RNA complex appeared to be less α-helical.

NMR Spectroscopy. NMR experiments can provide useful structural information about the boxB RNA and the N peptide, especially the structural change upon formation of the complex. In particular, imino protons from RNA base pairs in the stem and the Trp18 indole NH proton produce unique and easily detectable signals that are easy to monitor. NMR spectra were recorded to distinguish the boxB RNA binding between the acridine−peptide conjugate and the free peptide (Figure 4).

The free 15-mer boxB RNA (Figure 4A, a) has 5 bp in the stem. The 1D imino proton NMR spectrum showed three peaks (13.25, 12.65, and 12.55 ppm) corresponding to the imino protons of G12, G13, and G14 from the three middle CG base pairs. The terminal GC pair was not observable due to fraying, and the U

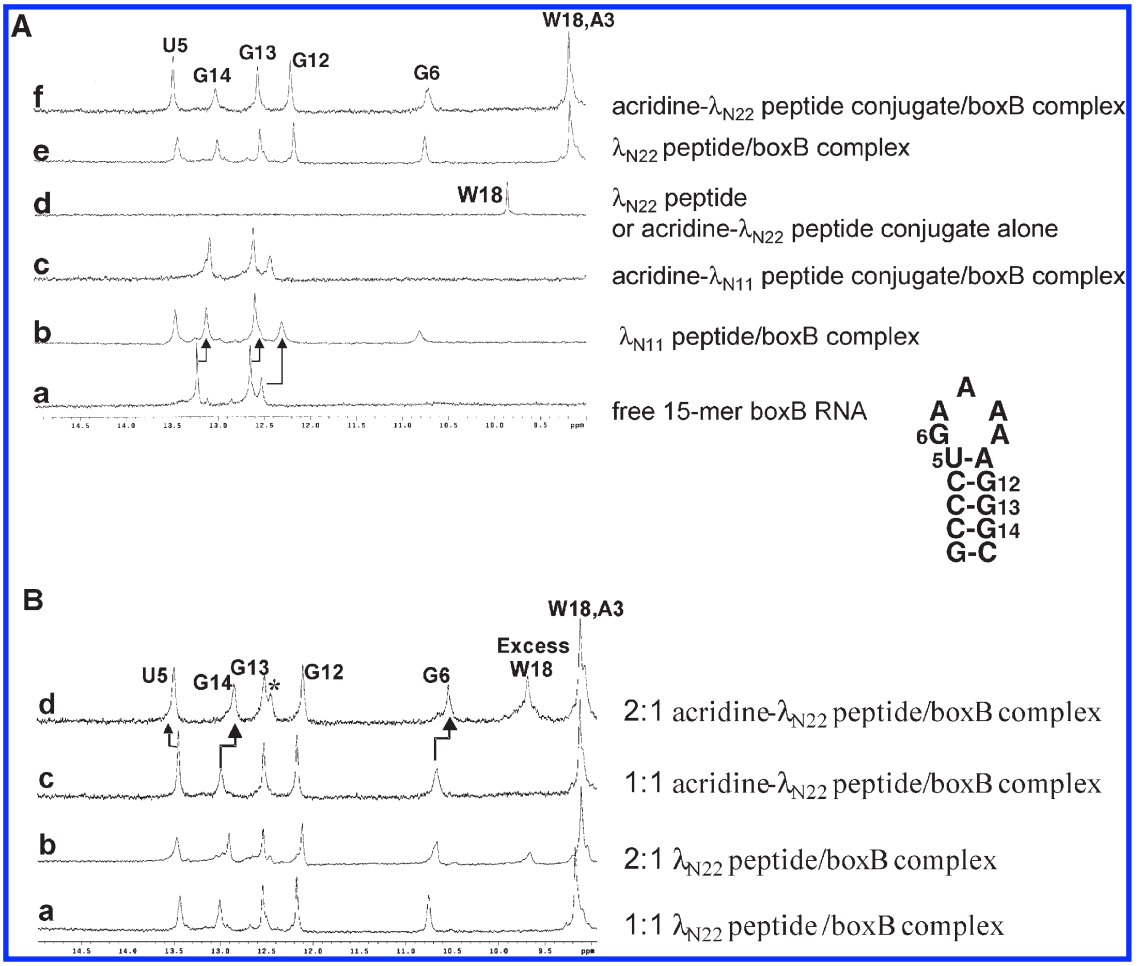

FIGURE 4: One-dimensional NMR spectra for the peptide, boxB RNA, and complexes. (A) Comparison of λ_{N11} and λ_{N22} peptide−boxB complexes: (a) free 15-mer boxB RNA, (b) λ_{N11} peptide−boxB complex, (c) acridine−λ_{N11} peptide conjugate−boxB RNA complex, (d) λ_{N22} peptide or acridine−λ_{N22} peptide conjugate alone, (e) λ_{N22} peptide−boxB RNA complex, and (f) acridine−λ_{N22} peptide conjugate−boxB complex. (B) Comparison of the 1:1 peptide−boxB complex and the 2:1 peptide−boxB complex: (a) 1:1 λ_{N22} peptide−boxB complex, (b) 2:1 λ_{N22} peptide−boxB complex, (c) 1:1 acridine−λ_{N22} peptide conjugate−boxB RNA complex, and (d) 2:1 acridine−λ_{N22} peptide conjugate−boxB RNA complex. The asterisk indicates the additional peak.

imino proton from the loop closing UA pair was also missing, presumably because of the flexibility of the unstructured penta-loop in the free RNA. Binding by either full-length N peptide or truncated amino-terminal 11-mer induced similar RNA structural changes, evidenced by shifting of the three CG imino protons to higher field (Figure 4A, b and e). Beside these changes, there were additional imino protons at 13.5 ppm corresponding to U5 of the UA pair and a broader peak at 10.7 ppm attributable to the G6 imino proton from the sheared GA base pair characteristic of the GNRA tetraloop type of folding. This indicates that the loop has been stabilized by peptide binding. In addition, the Trp18 indole NH proton in the full-length peptide has a large shift from 10 ppm (Figure 4A, d) in the free peptide to 9.2 ppm in the complex (Figure 4A, e), which is due to the stacking interaction between Trp18 and the RNA loop (*30*).

In comparison, the spectrum for the acridine−linker **2**−λ_{N11} conjugate bound to the boxB RNA (Figure 4A, c) did not show these characteristic signal changes as observed for the λ_{N11} peptide−RNA complex, except for the broadening of the three original peaks. This indicated that the acridine−λ_{N11} peptide conjugate did not bind the RNA in the same mode as the λ_{N11} peptide. Since acridine compound 3-acridin-9-ylaminopropanol was found to bind to the boxB RNA with an affinity of ~15 μM, similar to the affinity between the λ_{N11} peptide and the boxB RNA, it is possible that the two modules compete for the RNA binding site, and the acridine moiety may associate with the RNA nonspecifically, thus disrupting the specific complex structure between the λ_{N11} peptide and the boxB RNA. The imino protons of U5 and G6 are therefore broadened because of the heterogeneity of the complex, as observed in other cases (*41*).

The spectrum for the 1:1 acridine−linker **2**−full-length peptide conjugate−boxB RNA complex (Figure 4A, f) showed very similar imino proton signals for the RNA component and the characteristic Trp18 indole proton shift as seen in the spectrum for the λ_{N22} peptide complex. Within the acridine−full-length peptide conjugate, the peptide portion appeared to bind the RNA in the same mode as in the wild-type λ_{N22} peptide−RNA complex, thus delivering the acridine moiety to the lower part of boxB RNA stem.

Since the acridine−full-length peptide conjugate exhibited biphasic binding to the boxB RNA, we further investigated the potential second binding site on the boxB RNA for the conjugate. Overtitration of the conjugate produced a 2:1 ratio for the conjugate−RNA complex. Comparison of the spectra for 1:1 and 2:1 complexes of both the WT peptide and the acridine−peptide conjugate revealed interesting discrepancies (Figure 4B). The imino protons for U5 moved further downfield, and G6 and G14 moved upfield; furthermore, there was an additional peak at

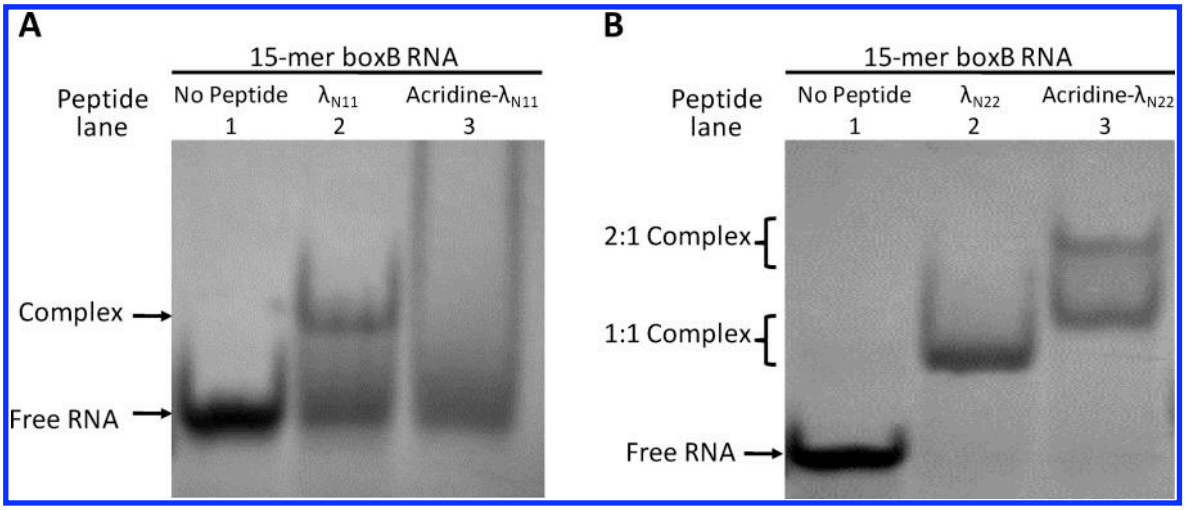

FIGURE 5: Gel shift analysis of peptide−boxB RNA complexes for WT peptides and acridine−peptide conjugates. (A) λ_{N11}−RNA and acridine−λ_{N11}−RNA complexes. (B) λ_{N22}−RNA and acridine−λ_{N22}−RNA complexes.

12.4 ppm. These features suggest a specific second binding site for the acridine−peptide conjugate.

Band Shift Analysis. Observations from NMR experiments were consistent with the band shift analysis shown in Figure 5. A band shift was observed indicative of specific binding of the boxB RNA by the λ_{N11} peptide (lane 2 of Figure 5A). On the other hand, the smear for the acridine−linker **2**−λ_{N11} peptide conjugate with the boxB RNA (lane 3 of Figure 5A) indicated nonspecific interaction, possibly random intercalation of acridine either in the stem or in the loop region which competes with the binding of the peptide portion.

The acridine−linker **2**−λ_{N22} full-length conjugate, however, exhibited not only a 1:1 complex with the boxB RNA 15-mer (lane 3 of Figure 5B) as in the peptide−RNA complex (lane 2 of Figure 5B) but also a higher-stoichiometry complex as well. These results, likely suggestive of a second binding site for the acridine−λ_{N22} peptide conjugate, may explain the profile of the fluorescence titration curves, which sometimes show biphasic transitions with the second transition apparently following equimolar titration.

DISCUSSION

To achieve higher RNA binding affinities, the design of a ligand consisting of two moieties connected by a linker is a promising approach (*8*, *9*). Higher binding affinities could result from a favorable entropic factor compared with the binding of the two monomeric counterparts. Under certain conditions, the length and nature of the linker are critical. The molecule can be a dimeric form of a known binder (*42*) or consist of two distinct moieties that bind to RNA in different modes, e.g., groove binding and intercalation (*15*−*18*). To apply this idea to the N peptide system, we designed and synthesized a series of λN peptide-based peptide−acridine conjugates. Their binding affinities for boxB RNAs with stem−loop hairpin structures were determined by steady-state fluorescence measurements.

Binding Affinity and Specificity Enhancement. Acridine compound 3-acridin-9-ylaminopropanol binds the boxB RNA with an affinity of 15 μM, potentially conferring significant enhancement when linked to another binding module. From a comparison of the salt dependence of binding, our acridine−linker **2**−λ_{N22} peptide conjugation showed 80-fold binding enhancement over a broad range of salt concentrations. This result is similar to the binding enhancement observed for a neo-acridine construct over neomycin B alone binding to a RRE RNA (*18*). This observed binding enhancement was unique to the full-length conjugate with a more flexible ethylene glycol linker tested, implying that the structural context of acridine presentation was critical. The same construct showed only 3-fold tighter binding to a related P22 boxB RNA target. Compared to λ boxB, P22 RNA displays a flipped orientation for one base pair in the stem and has a cytidine in the loop instead of adenine (Table 1). Homologous hydrophobic interactions occur between the boxB hairpin stem and conserved alanine residues within the N peptide amino-terminal module. Distinct hydrophobic interactions are involved between the boxB hairpin loops and carboxy-terminal modules of the N peptides. In λ, a tryptophan residue stacks on the boxB loop; in P22, nonpolar alanine and isoleucine residues interact with an extruded pyrimidine. In both phage λ and P22, the bound pentaloops adopt stable GNRA tetraloop folds by extruding either loop base 4 (4-out) in the λ complex or loop base 3 (3-out) in the P22 complex. Both λ_{N22} and $P22_{N21}$ full-length peptides discriminate strongly between their cognate RNA hairpins and other boxB RNA targets (*34*, *38*). Our acridine−linker **2**−λ_{N22} peptide conjugate exhibited 25-fold binding specificity enhancement between these two similar RNA structures.

In contrast, the acridine−λ_{N11} peptide conjugate displayed 3-fold weaker binding than the λ_{N11} peptide alone. The NMR and gel shift data showed that the conjugate did not form a specific complex with the boxB RNA (Figures 4A and 5A), presumably due to the fact that the nonspecific binding of the acridine moiety to the boxB RNA showed an affinity similar to that of the λ_{N11} peptide. Therefore, the acridine moiety competed with the peptide moiety for RNA binding sites. Alternatively, it is also possible that in the acridine−λ_{N11} conjugate, nonspecific electrostatic attraction by Arg residues in the peptide to the RNA becomes important as the origin of the low binding affinity of the acridine−λ_{N11} conjugate. This result suggests that when a ligand with multiple binding modules is designed, it is important to avoid a nonspecific binding module that can compete for binding to multiple sites intended for other modules. Furthermore, a module with a higher affinity for one site will help anchor the entire ligand. Taken together, our observations indicate that the specific binding peptide module of the full-length acridine−peptide conjugate exhibits a much higher affinity for the λboxB RNA,

thereby maintaining the native contacts with RNA (Figure 4A) and facilitating delivery of the acridine moiety to the intended site.

Acridine Intercalating Site. Previous structural studies on DNA intercalated with acridine-related compounds have consistently shown intercalation sites at alternating base steps, particularly at the terminal base steps (*43*). This is likely due to the fact that terminal base steps have much greater conformational freedom than internal base steps and, thus, are more receptive to intercalation. Recent studies on DACA, an antitumor acridine derivatized with variable functional substitutions at position 4, showed that they intercalate into DNA with side chains positioned in the major groove (*44*−*46*). However, the crystal structure of an acridine−tetraarginine conjugate with the peptide attached to position 9 showed intercalation of acridine into the minor groove of the central AA/TT base step of a long DNA fragment, leaving the peptide in the minor groove (*47*).

In these cases, it appeared that specific hydrogen bonding interactions between the lateral chain of acridine and DNA may affect how the acridine moiety intercalates into nucleic acid. Interestingly, a recent study also showed that in peptide−acridine conjugates, the point of attachment on acridine affected the conjugates' affinity for the nucleic acid target (*11*).

Our acridine−N peptide conjugates feature attachment of the peptide to acridine at position 9, similar to the acridine−tetraarginine case. The mode of binding of acridine in these conjugates is currently unknown. If the acridine moiety derivatized at position 9 with a peptide prefers intercalation into the minor groove as in the case of the acridine−tetraarginine complex (*47*), our construct may preclude intercalation because the full-length N peptide binds to the boxB RNA in the major groove with high affinity. With respect to the acridine−λ_{N11} conjugate, the acridine may be able to intercalate into the minor groove; however, such intercalation is probably not site-specific. Alternatively, binding of the N peptide, especially the full-length version, to the boxB RNA peptide may induce RNA folding. There are extensive interactions between the peptide and the RNA stem, some of which may be disrupted by an intercalated acridine moiety in the stem. Although the acridine may still be able to intercalate at the terminal base step, the inability to directly observe the imino proton from the terminal base pair precludes direct confirmation of this possibility.

A Second Specific Binding Site for the Acridine−*N Peptide Conjugate on the boxB RNA*. Similar to the neo-acridine case (*18*) which involved a second binding site, our fluorescence, NMR, and gel shift data also suggested a second specific binding site for the acridine−N peptide conjugate on the boxB RNA. The nature of the second site is not known but may involve either the major or the minor groove. Changes in the imino proton chemical shifts were observed throughout the RNA structure (Figures 4B and 5), suggesting extensive interactions.

Alternative approaches to enhancing RNA binding affinity are also available. N peptides bind to the boxB RNA in an α-helical conformation but exhibit little helical structure when free in solution (*31*). Stabilizing the helical form of such peptides is expected to favor RNA binding by virtue of preorganization. For example, C^{α}-substituted amino acids have long been recognized as a means of introducing local conformational restriction into peptides (*48*). Another approach to stabilize the α-helical form of peptides is through the incorporation of covalent linkages between constituent amino acid side chains. It was found that substantial helix stabilization was achieved when the linkage was placed between residues i and $i + 4$ in the peptide backbone by ring closing metathesis (*49*−*52*). Therefore, cyclic helical N peptides in which ring closing metathesis is used to incorporate a carbon−carbon tether between appropriate residue side chains is expected to enhance binding. In line with this view, our analyses revealed that the full-length peptide−acridine conjugate had substantially improved RNA binding affinity (∼80-fold) and specificity (∼25-fold) relative to those of the peptide alone. Our work supports the idea that peptide- and intercalation-based binding can be combined to create a new class of high-affinity, high-specificity RNA-binding ligands. This approach provides straightforward optimization to enhance the affinity of known modules and facilitate the discovery of powerful new hybrid ligands with novel functionalities.

ACKNOWLEDGMENT

We thank Drs. T. T. Takahashi and Ryan J. Austin for helpful discussions.

REFERENCES

1. Klug, A. (1999) Zinc finger peptides for the regulation of gene expression. *J. Mol. Biol. 293*, 215–218.
2. Segal, D. J., and Barbas, C. F., III (2000) Design of novel sequence-specific DNA-binding proteins. *Curr. Opin. Chem. Biol. 4*, 34–39.
3. Wolfe, S. A., Nekludova, L., and Pabo, C. O. (2000) DNA recognition by Cys2His2 zinc finger proteins. *Annu. Rev. Biophys. Biomol. Struct. 29*, 183–212.
4. White, S., Szewczyk, J. W., Turner, J. M., Baird, E. E., and Dervan, P. B. (1998) Recognition of the four Watson-Crick base pairs in the DNA minor groove by synthetic ligands. *Nature 391*, 468–471.
5. Dervan, P. B. (2001) Molecular recognition of DNA by small molecules. *Bioorg. Med. Chem. 9*, 2215–2235.
6. Fechter, E. J., and Dervan, P. B. (2003) Allosteric inhibition of protein−DNA complexes by polyamide−intercalator conjugates. *J. Am. Chem. Soc. 125*, 8476–8485.
7. Fechter, E. J., Olenyuk, B., and Dervan, P. B. (2004) Design of a sequence-specific DNA bisintercalator. *Angew. Chem., Int. Ed. 43*, 3591–3594.
8. Michael, K., and Tor, Y. (1998) Designing novel RNA binders. *Chem. Eur. J. 4*, 2091–2098.
9. Cheng, A. C., Calabro, V., and Frankel, A. D. (2001) Design of RNA-binding proteins and ligands. *Curr. Opin. Struct. Biol. 11*, 478–484.
10. Pushechnikov, A., Lee, M. M., Childs-Disney, J. L., Sobczak, K., French, J. M., Thornton, C. A., and Disney, M. D. (2009) Rational Design of Ligands Targeting Triplet Repeating Transcripts That Cause RNA Dominant Disease: Application to Myotonic Muscular Dystrophy Type 1 and Spinocerebellar Ataxia Type 3. *J. Am. Chem. Soc. 131*, 9767–9779.
11. Carlson, C. B., and Beal, P. A. (2002) Point of attachment and sequence of immobilized Peptide-acridine conjugates control affinity for nucleic acids. *J. Am. Chem. Soc. 124*, 8510–8511.
12. Carlson, C. B., Spanggord, R. J., and Beal, P. A. (2002) Selection of small-molecule mediators of the RNA regulation of PKR, the RNA-dependent protein kinase. *ChemBioChem 3*, 859–865.
13. Carlson, C. B., Vuyisich, M., Gooch, B. D., and Beal, P. A. (2003) Preferred RNA binding sites for a threading intercalator revealed by in vitro evolution. *Chem. Biol. 10*, 663–672.
14. Gooch, B. D., and Beal, P. A. (2004) Recognition of duplex RNA by helix-threading peptides. *J. Am. Chem. Soc. 126*, 10603–10610.
15. Hamy, F., Brondani, V., Florsheimer, A., Stark, W., Blommers, M. J., and Klimkait, T. (1998) A new class of HIV-1 Tat antagonist acting through Tat-TAR inhibition. *Biochemistry 37*, 5086–5095.
16. Wilson, W. D., Ratmeyer, L., Cegla, M. T., Spychala, J., Boykin, D., Demeunynck, M., Lhomme, J., Krishnan, G., Kennedy, D., Vinayak, R., and Zon, G. (1994) Bulged-base nucleic acids as potential targets for antiviral drug action. *New J. Chem. 18*, 419–423.
17. Wilson, W. D., Mizan, S., Tanious, F. A., Yao, S., and Zon, G. (1994) The interaction of intercalators and groove-binding agents with DNA triple-helical structures: The influence of ligand structure, DNA backbone modifications and sequence. *J. Mol. Recognit. 7*, 89–98.
18. Kirk, S. R., Luedtke, N. W., and Tor, Y. (2000) Neomycin-acridine conjugate: A potent inhibitor of Rev-RRE binding. *J. Am. Chem. Soc. 122*, 980–981.

19. Tung, C. H., Wei, Z., Leibowitz, M. J., and Stein, S. (1992) Design of peptide-acridine mimics of ribonuclease activity. *Proc. Natl. Acad. Sci. U.S.A. 89*, 7114–7118.
20. Fkyerat, A., Demeunynck, M., Constant, J.-F., Michon, P., and Lhomme, J. (1993) A New Class of Artificial Nucleases That Recognize and Cleave Apurinic Sites in DNA with Great Selectivity and Efficiency. *J. Am. Chem. Soc. 115*, 9952–9959.
21. Kuzuya, A., Mizoguchi, R., Morisawa, F., Machida, K., and Komiyama, M. (2002) Metal ion-induced site-selective RNA hydrolysis by use of acridine-bearing oligonucleotide as cofactor. *J. Am. Chem. Soc. 124*, 6887–6894.
22. Greenblatt, J., Nodwell, J. R., and Mason, S. W. (1993) Transcriptional antitermination. *Nature 364*, 401–406.
23. Das, A. (1993) Control of transcription termination by RNA-binding proteins. *Annu. Rev. Biochem. 62*, 893–930.
24. Salstrom, J. S., and Szybalski, W. (1978) Coliphage λnutL-: A unique class of mutants defective in the site of gene N product utilization for antitermination of leftward transcription. *J. Mol. Biol. 124*, 195–221.
25. Olson, E. R., Tomich, C. S., and Friedman, D. I. (1984) The nusA recognition site. Alteration in its sequence or position relative to upstream translation interferes with the action of the N antitermination function of phage λ. *J. Mol. Biol. 180*, 1053–1063.
26. Lazinski, D., Grzadzielska, E., and Das, A. (1989) Sequence-specific recognition of RNA hairpins by bacteriophage antiterminators requires a conserved arginine-rich motif. *Cell 59*, 207–218.
27. Barrick, J. E., Takahashi, T. T., Ren, J., Xia, T., and Roberts, R. W. (2001) Large libraries reveal diverse solutions to an RNA recognition problem. *Proc. Natl. Acad. Sci. U.S.A. 98*, 12374–12378.
28. Heus, H. A., and Pardi, A. (1991) Structural features that give rise to the unusual stability of RNA hairpins containing GNRA loops. *Science 253*, 191–194.
29. Legault, P., Li, J., Mogridge, J., Kay, L. E., and Greenblatt, J. (1998) NMR structure of the bacteriophage λ N peptide/boxB RNA complex: Recognition of a GNRA fold by an arginine-rich motif. *Cell 93*, 289–299.
30. Scharpf, M., Sticht, H., Schweimer, K., Boehm, M., Hoffmann, S., and Rosch, P. (2000) Antitermination in bacteriophage λ. The structure of the N36 peptide-boxB RNA complex. *Eur. J. Biochem. 267*, 2397–2408.
31. Su, L., Radek, J. T., Hallenga, K., Hermanto, P., Chan, G., Labeots, L. A., and Weiss, M. A. (1997) RNA recognition by a bent α-helix regulates transcriptional antitermination in phage λ. *Biochemistry 36*, 12722–12732.
32. Lacourciere, K. A., Stivers, J. T., and Marino, J. P. (2000) Mechanism of neomycin and Rev peptide binding to the Rev responsive element of HIV-1 as determined by fluorescence and NMR spectroscopy. *Biochemistry 39*, 5630–5641.
33. Kuzmic, P. (1996) Program DYNAFIT for the analysis of enzyme kinetic data: Application to HIV proteinase. *Anal. Biochem. 237*, 260–273.
34. Austin, R. J., Xia, T., Ren, J., Takahashi, T. T., and Roberts, R. W. (2003) Differential modes of recognition in N peptide-boxB complexes. *Biochemistry 42*, 14957–14967.
35. Milligan, J. F., Groebe, D. R., Witherell, G. W., and Uhlenbeck, O. C. (1987) Oligoribonucleotide synthesis using T7 RNA polymerase and synthetic DNA templates. *Nucleic Acids Res. 15*, 8783–8798.
36. Menger, M., Eckstein, F., and Porschke, D. (2000) Dynamics of the RNA hairpin GNRA tetraloop. *Biochemistry 39*, 4500–4507.
37. Rachofsky, E. L., Osman, R., and Ross, J. B. (2001) Probing structure and dynamics of DNA with 2-aminopurine: Effects of local environment on fluorescence. *Biochemistry 40*, 946–956.
38. Austin, R. J., Xia, T., Ren, J., Takahashi, T. T., and Roberts, R. W. (2002) Designed arginine-rich RNA-binding peptides with picomolar affinity. *J. Am. Chem. Soc. 124*, 10966–10967.
39. Record, M. T., Jr., Lohman, M. L., and De Haseth, P. (1976) Ion effects on ligand-nucleic acid interactions. *J. Mol. Biol. 107*, 145–158.
40. Record, M. T., Jr., Ha, J. H., and Fisher, M. A. (1991) Analysis of equilibrium and kinetic measurements to determine thermodynamic origins of stability and specificity and mechanism of formation of site-specific complexes between proteins and helical DNA. *Methods Enzymol. 208*, 291–343.
41. Robertson, S. A., Harada, K., Frankel, A. D., and Wemmer, D. E. (2000) Structure determination and binding kinetics of a DNA aptamer-argininamide complex. *Biochemistry 39*, 946–954.
42. Campisi, D. M., Calabro, V., and Frankel, A. D. (2001) Structure-based design of a dimeric RNA-peptide complex. *EMBO J. 20*, 178–186.
43. Williams, L. D., Egli, M., Gao, Q., and Rich, A., Eds. (1992) Nucleic Acids, Vol. *I*, Adenine Press, Schenectady, NY.
44. Todd, A. K., Adams, A., Thorpe, J. H., Denny, W. A., Wakelin, L. P., and Cardin, C. J. (1999) Major groove binding and 'DNA-induced' fit in the intercalation of a derivative of the mixed topoisomerase I/II poison N-(2-(dimethylamino)ethyl)acridine-4-carboxamide (DACA) into DNA: X-ray structure complexed to d(CG(5-BrU)ACG)2 at 1.3-Å resolution. *J. Med. Chem. 42*, 536–540.
45. Adams, A., Guss, J. M., Denny, W. A., and Wakelin, L. P. (2002) Crystal structure of 9-amino-N-[2-(4-morpholinyl)ethyl]-4-acridinecarboxamide bound to $d(CGTACG)_2$: Implications for structure-activity relationships of acridinecarboxamide topoisomerase poisons. *Nucleic Acids Res. 30*, 719–725.
46. Adams, A., Guss, J. M., Collyer, C. A., Denny, W. A., and Wakelin, L. P. (1999) Crystal structure of the topoisomerase II poison 9-amino-[N-(2-dimethylamino)ethyl]acridine-4-carboxamide bound to the DNA hexanucleotide $d(CGTACG)_2$. *Biochemistry 38*, 9221–9233.
47. Malinina, L., Soler-Lopez, M., Aymami, J., and Subirana, J. A. (2002) Intercalation of an Acridine-Peptide Drug in an AA/TT Base Step in the Crystal Structure of $[d(CGCGAATTCGCG)]_2$ with Six Duplexes and Seven Mg^{2+} Ions in the Asymmetric Unit. *Biochemistry 41*, 9341–9348.
48. Liff, M. I., Kopple, K. D., Tian, Z., and Roeske, R. W. (1994) Effects of C α-methyl substitution on the conformation of linear GnRH antagonist analogs. *Int. J. Pept. Protein Res. 43*, 471–476.
49. Miller, S. J., and Grubbs, R. H. (1995) Synthesis of Conformationally Restricted Amino-Acids and Peptides Employing Olefin Metathesis. *J. Am. Chem. Soc. 117*, 5855–5856.
50. Lynn, D. M., Mohr, B., and Grubbs, R. H. (1998) Living ring-opening metathesis polymerization in water. *J. Am. Chem. Soc. 120*, 1627–1628.
51. Blackwell, H. E., and Grubbs, R. H. (1998) Highly efficient synthesis of covalently cross-linked peptide helices by ring-closing metathesis. *Angew. Chem., Int. Ed. 37*, 3281–3284.
52. Schafmeister, C. E., Po, J., and Verdine, G. L. (2000) An all-hydrocarbon cross-linking system for enhancing the helicity and metabolic stability of peptides. *J. Am. Chem. Soc. 122*, 5891–5892.